Quantification of cloud water interception along the windward slope of Santa Cruz Island, Galapagos (Ecuador)

Alexandre Pryet, Christian Dominguez, Pilar Fuente Tomai, Cédric Chaumont, Marcos Villacis, Noémi d'Ozouville, Sophie Violette

Quantification of cloud water interception along the windward slope of Santa Cruz Island, Galapagos (Ecuador)

Alexandre Pryet[a,], Christian Dominguez[b], Pilar Fuente Tomai[a,c], Cédric Chaumont[d], Noémi d'Ozouville[a], Marcos Villacís[b], Sophie Violette[a]

[a] *UPMC Univ. Paris 6 & CNRS, UMR Sisyphe, 4 place Jussieu, 75252 Paris cedex 05, France*

[b] *Department of Civil and Environmental Engineering, National Polytechnic School, Quito, Ecuador*

[c] *Department of Silviculture and Pastures, Forest Engineering School, University Polytechnic of Madrid, Spain*

[d] *CEMAGREF Antony, France*

Abstract

The Galapagos Archipelago is nearly devoid of freshwater resources, but during six months of the year, a fog layer covers the windward slopes of the main islands. In order to investigate the hydrological importance of this phenomenon, a monitoring network was set up on Santa Cruz Island, at the center of the archipelago. Meteorological parameters were monitored together with throughfall and stemflow at two stations: a first in a secondary forest at the lowest fringe of the fog layer (400 m a.s.l.), and a second in shrub lands of the Galapagos National Park, at the center of the fog layer (650 m a.s.l.). Cloud water interception was quantified from the wet canopy water budget, based on a modified *Rutter*-type canopy interception model. This methodology allowed the estimation of fog interception for short time intervals (15 min) and avoided the subjective separation into individual rainfall events. Fog was found to be a negligible water input at the lower site, but contributed up to 26 $\pm$ 16% of incident rainfall at the higher site. Wind was shown to enhance fog interception, but this alone could not explain the difference in fog catch between the two sites. Higher liquid water content and more frequent fog occurrence contributed to the difference as well. This study highlights that the presence of fog may induce a marked increase of net precipitation, but this effect is restricted to the summit areas exposed to winds, located in the center of the cloud belt.

dx.doi.org/10.1016/j.agrformet.2012.03.018

Keywords:
Cloud Water Interception, Fog, Throughfall, Galapagos

Email address: a.pryet@gmail.com (Alexandre Pryet)
Published in Agricultural and Forest Meteorology 161 (2012) 94-106

1. Introduction

The interception of wind-blown droplets of water by the vegetation, commonly called *cloud water interception* (*CWI*) can be a significant input to the canopy water budget. Previous studies reported fog contributions ranging between 2% and 45% of incident annual rainfall (Bruijnzeel, 2001; Bruijnzeel et al., 2011). This phenomenon occurs during conditions of low vapor pressure deficits and weak solar radiation and is therefore associated with limited potential evapotranspiration (Bruijnzeel, 2001; Ritter et al., 2009). Together, these processes provide optimal conditions for groundwater recharge and streamflow generation. Climate change could result in a raising of cloud base (Still et al., 1999; Foster, 2001). Deforestation may reduce cloud occurrence, and cloud water interception by the vegetation (Bruijnzeel, 2001; Brauman et al., 2010; Lawton et al., 2001). For regions where water resources are limited and fog occurrence is frequent, it is of the highest importance to quantify fog interception and identify its controlling processes (Bruijnzeel et al., 2011).

Air liquid water content, wind speed, and canopy structure have been identified as the main driving factors of fog interception (Bruijnzeel, 2001; Bruijnzeel et al., 2005). *CWI* can not be measured directly, because rain gauges do not intercept horizontal wind-blown droplets of water, while artificial fog gauges do not provide a direct quantification of *CWI* by the vegetation (Holwerda et al., 2006a, 2011). The quantification of *CWI* thus requires the measurement of throughfall and stemflow, the two components of net precipitation, along with wet canopy evaporation. The direct measurement of evaporation remains challenging even with sophisticated eddy-covariance instrumentation (Gash et al., 1999; Holwerda et al., 2012). Recent advances have presented the wet canopy water budget as the most promising method to quantify fog interception (Bruijnzeel et al., 2011; Holwerda et al., 2006a). This method uses the difference between measured and modelled net precipitation to quantify cloud water interception. Recent applications are numerous, most of them are based on *Gash*-type (Gash, 1979), event-based interception models (e.g. Giambelluca et al. (2011); Holwerda et al. (2010a,b); McJannet et al. (2007b) and Muñoz-Villers et al. (2011)), few of them used a *Rutter*-type (Rutter et al., 1972), running water budget interception model (e.g. Takahashi et al. (2011)).

The occurrence of fog is reported in many oceanic islands and has been investigated by several recent studies such as in Hawaii (US) (Brauman et al., 2010; Giambelluca et al., 2011; Takahashi et al., 2011), La Réunion Is-

land (France) (Gabriel and Jauze, 2008), Madeira Island (Portugal) (Prada et al., 2009), and Canary Islands (Spain) (García-Santos and Bruijnzeel, 2011).

In the Galapagos Islands, a semi-permanent fog layer covers the highlands during the cool *garúa* season, from June to December (Trueman and d'Ozouville, 2010). The fog has been shown to have an effect on local ecosystems (Jäger et al., 2009), but its contribution to the water budget has never been investigated. As described by pioneering authors, the archipelago is nearly devoid of freshwater (Porter, 1815; Darwin, 1859). With the rapid human population growth related to the tourism industry, there is an increasing demand for freshwater. The current situation is critical and local population relies on expensive desalination techniques (d'Ozouville, 2007a,b; INEC-CGG, 2010). There is a need for a better understanding of the local hydrology.

This paper presents the results of investigations performed along the windward side of Santa Cruz Island during the 2010 fog *garúa* season, and provides the first quantitative estimation of fog interception in the Galapagos Archipelago.

2. Study Area

2.1. Regional climatic context

The Galapagos Islands lie 1000 km west of the South-American coasts in the Pacific Ocean, straddling the Equator. The climate is oceanic, with sea surface and air temperatures being anomalously low due to upwelling of the cold Equatorial and *Humboldt* ocean-currents (Eden and Timmermann, 2004). Extreme inter-annual climatic variations observed in the islands are related to the *El Niño Southern Oscillation* (ENSO). The *El Niño* events are expressed by marked increase in precipitations while their opposite counterparts, the *La Niña* events, are characterized by a drop in precipitation and often correspond to years of drought (Snell and Rea, 1999).

Similarly to the situation in the Hawaiian Archipelago (Giambelluca and Nullet, 1991; Nullet et al., 1995; Kolivras and Comrie, 2007), the orographic lifting of moist air driven by trade-winds induces clear discrepancies between the humid windward slopes subjected to orographic precipitation, and the arid leeward slopes deprived of water by the rain shadow effect. Seasons alternate between a hot *invierno* season (January to May) and a cooler *garúa* season (June to December). During the hot *invierno* season, rainfall is convective, with the amount of precipitation positively correlated

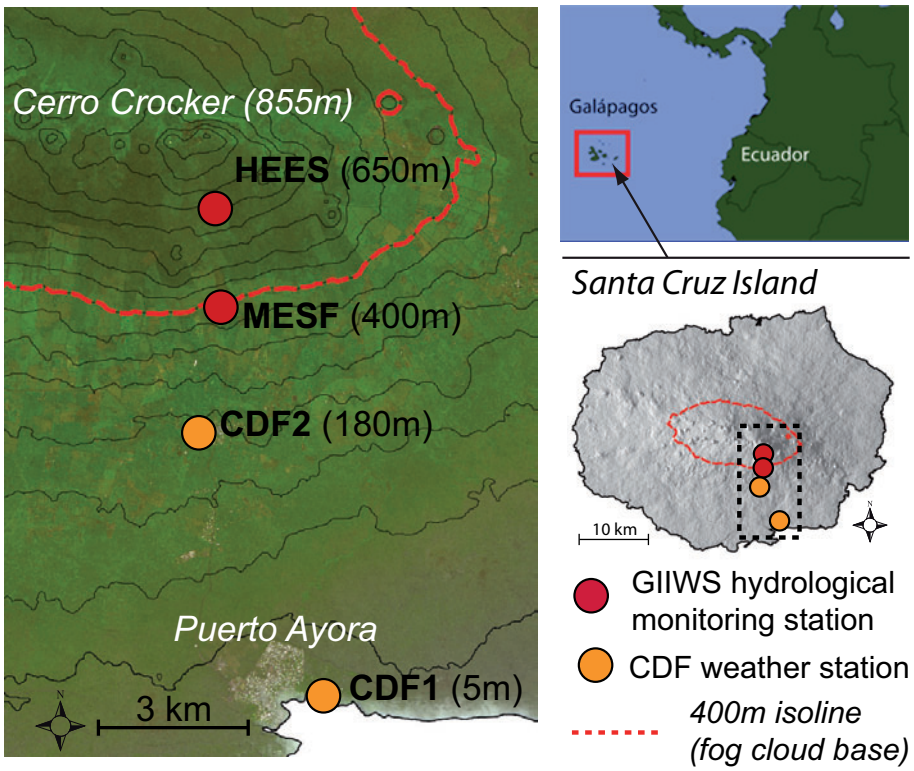

Figure 1: Santa Cruz Island, at the center of Galapagos Archipelago (Ecuador) (©CNES-SPOT image). CDF1 and CDF2 are weather stations operated by the Charles Darwin Foundation (CDF). MESF, and HEES are the two hydrological monitoring stations set up for this study, in the frame of the project *Galapagos Island integrated Water Studies* (GIIWS).

with sea surface temperatures (Trueman and d'Ozouville, 2010). During the cool *garúa* season, an inversion layer is formed, which hampers the further rise of moist air and leads to the formation of fog in the highlands. This phenomenon is observed on all the islands above ca. 400 m a.s.l. (Sachs and Ladd, 2010; Trueman and d'Ozouville, 2010). Current meteorological patterns in the Galapagos may be affected in future by the consequences of climate change (Sachs and Ladd, 2010). The frequency of fog occurrence could be reduced and the cloud base level raised. However, another possibility is more frequent occurrence of the *La Niña* anomalies, which favor fog occurrence.

2.2. Climatic and vegetation zonation of Santa Cruz Island

Santa Cruz island lies at the center of the archipelago (Fig. 1), it is the second largest (986 km^2) and the most populated island with officially 13,000 inhabitants (INEC-CGG, 2010). It is the center of touristic activity in the archipelago, which receives a yearly flux of 173,000 tourists (PNG, 2010). Santa Cruz is characterized by a broad low elevation coastal apron surrounding a main central shield culminating at *Cerro Crocker*, 855 m a.s.l. (d'Ozouville et al., 2008).

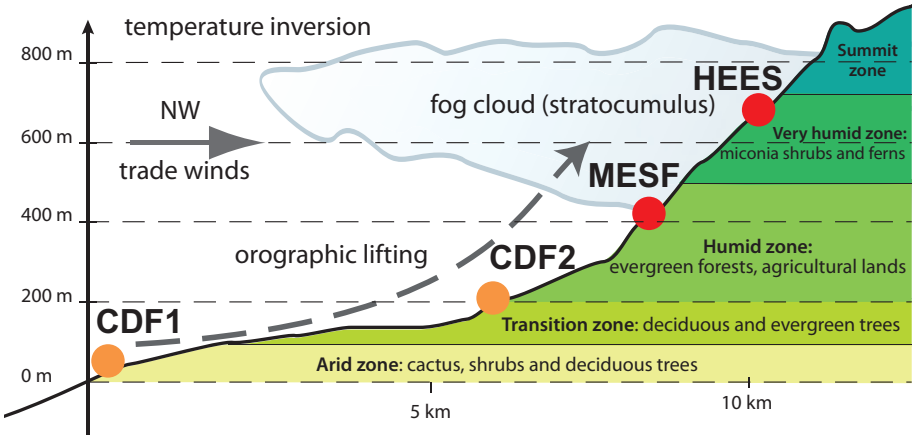

Figure 2: Vegetation zoning along the windward slope of Santa Cruz island after Hamann (1979). The four weather stations (CDF1, CDF2, MESF, HEES) highlight the contrasting climatic conditions at the origin of the vegetation zonation.

Two long-term weather stations are operated by the *Charles Darwin Foundation* (CDF). The first (hereafter called CDF1) is located in Puerto

Ayora (5 m a.s.l.) and the second (hereafter called CDF2) in Bellavista (alt. 180 m a.s.l.) (Fig. 1). They have been operational since 1964 and 1987, respectively. Recorded median annual rainfall totals are 277 mm and 800 mm, respectively. The coastal station (CDF1) receives the major part of annual precipitation during the convective rains of the hot *invierno* season. This is the opposite at the second station, where most of the rainfall is recorded during the cool *garúa* season (Trueman and d'Ozouville, 2010). As described by the seasonal isohyet maps proposed by Trueman and d'Ozouville (2010), the spatial distribution of rainfall varies with seasons. Due to the orographic effect, contrasts are more acute during the *garúa* season, when the fog layer is observed along the windward slope from 300-400 m a.s.l. up to the summit (Trueman and d'Ozouville, 2010). The summit area occasionally remains clear of clouds, but the upper limit of the fog layer (the inversion layer) is most often above the top of the island.

These contrasting climatic and physical conditions have induced a pronounced vegetation zonation along the windward side of the island (Fig. 2) (Hamann, 1979). From the coast up to 50 m a.s.l., conditions are arid, spiny shrubs and cactuses dominate. Between 50 m and 200 m a.s.l., vegetation progressively evolves to forests and soils are deeper. The humid zone extends from 200 to 450 m a.s.l. and was originally covered by the endemic *Scalesia* tree (Hamann, 1979). With the development of agriculture, the endemic forest has been replaced by alternates between pasture and secondary forest made up mainly by introduced trees species (*Psidium guajava*, *Cedrela odorata*, *Cinchona pubescens*). The very humid zone extends above 450 m a.s.l., soils are shallower and fractured basalt outcrops. The vegetation cover is composed of ferns and the endemic *Miconia robinsoniana* shrub. The area has been invaded by the *Cinchona pubescens* introduced in the 1940s (Jäger et al., 2009), but several control programs have markedly reduced its expansion. In the summit area, shrubs become scarce, fern and sedges dominate. Territories of the *Galapagos National Park* (GNP) extend from the top of the humid agricultural zone (ca. 450 m a.s.l.) up to the summit of the island, they are devoid of any agricultural activity.

Within the area covered by fog during the *garúa* season (i.e. from ca. 400 m a.s.l. to the summit), the vegetation of Santa Cruz Island presents typical characteristics of montane cloud forests (Bruijnzeel et al., 2011; Stadtmüller, 1987), with frequent vascular epiphytes and an abundance of non-vascular epiphytes (mosses) covering branches (Hamann, 1979). In the Galapagos Islands, fog occurs from a relatively low elevation with respect to other

montane cloud forests (Scatena et al., 2010). Given that trees and shrubs have a relatively short stature, the montane cloud forest of Santa Cruz Island area may therefore be classified as a *low-elevation elfin cloud forest* (Bruijnzeel et al., 2011; Scatena et al., 2010).

2.3. The two study plots

A first site (hereafter called MESF) was located at Mid-Elevation (400 m a.s.l.) beneath a Secondary Forest in the agricultural zone, where the dominant tree species are *Psidium guajava*, *Cestrum auriculatum*, and *Cinchona pubescens*. A second site (hereafter called HEES), was located at High-Elevation (650 m a.s.l.) beneath Endemic Shrubs (*Miconia robinsoniana*) of the very humid zone in the GNP park area (Figs. 1 and 2). At both sites, slopes are facing a south-south-east direction, but the slope is steeper at the HEES site (15°) than at the MESF site (10°) (Table 1).

Parameter	MESF	HEES
Long/Lat	90.32° W/0.67° S	90.32° W/0.65° S
Altitude [m a.s.l]	400	650
Slope	10°	15°
Aspect	170° E	160° E
Mean soil depth (range) [cm]	40 (8;90)	20 (5;30)
Vegetation type	Secondary forest	Evergreen shrub
Dominant tree species	*Psidium guajava*	*Miconia robinsoniana*
Mean canopy height [m]	5.45	2.8
Basal area [m^2/ha]	29.8	-
Stem density [stems/ha]	3550	-
LAI	4	2.7
Canopy gap fraction	19%	26%

Table 1: Physical conditions and characteristics of the vegetation at the two study plots. LAI and gap fractions were computed with the methodology described by Macfarlane et al. (2007).

Throughfall and stemflow measurements were performed within 6x6 m plots beneath vegetation canopy, while other meteorological instruments were installed in open areas in the vicinity. The interception of fog and wind-blown rain is known to be enhanced at the windward edges of vegetation patches (Weathers et al., 1995; Bruijnzeel et al., 2006). The location of each plot was chosen for measurements within the plots to be representative of the

Figure 3: The two instrumented study plots: secondary forest at the MESF plot (top) and the endemic *Miconia robinsoniana* shrubs at the HEES plot (bottom). Throughfall troughs drain into automatic tipping bucket gauges. Manually read throughfall and stemflow collectors were present at both plots but are only visible at the MESF plot (top panel, red and white arrows, respectively)

corresponding vegetation zones. The secondary forests of the agricultural zone occur in relatively large patches on gently sloping terrain, so that only a very limited portion of these forests is directly exposed to winds. The MESF plot was therefore located at the center of a relatively large (ca. 16 ha) forested patch, 40 m from a neighboring pasture. In contrast, the *Miconia* shrubs of the very humid zone grow on steeper slopes and form small patches varying in height. As a large proportion of the shrubs have a side exposed to winds, the HEES plot was located beneath a *Miconia* shrub with its southern edge exposed to winds.

Canopy coverage was characterized from photographs taken vertically (Dunkerley, 2010). A sufficient number of pictures were taken so as to cover fully the canopy overlying the study plots. These images were processed and converted into binary mode. The gap fraction of the canopy was estimated from the proportion of black pixels (Llorens and Gallart, 2000; Macfarlane et al., 2007). The leaf area index (LAI) was obtained from the methodology described by Macfarlane et al. (2007). For the albedo of the MESF plot, the value estimated by Giambelluca et al. (1999) for a secondary forest in northern Thailand was used (0.13). For the HEES plot, a value of 0.10 was assumed, as measured by Holwerda (2005) for a 2 m tall evergreen elfin cloud forest in Puerto Rico.

3. Materials and methods

3.1. Climate

Weather stations were placed in clearings close to the study plots (less than 100 m), but sufficiently distant to avoid perturbations. Measurements in open areas included rainfall, air temperature and relative humidity, wind speed and solar radiation. These variables were assumed to be representative of the conditions at the top of the canopy and were used for the estimation of potential evaporation (see Section 3.3 for details).

At the MESF plot, meteorological instruments were placed in a pasture adjacent to the forest, where the height of the grass varied between 0.4 m and 1 m. Solar radiation, relative humidity and temperature were measured at ca. 2 m above the ground, respectively, with a Kipp&Zonen SPLite silicone pyranometer and a Campbell CS215 T&RH sensor. Wind speed and direction were monitored with a Young WindSentry Kit composed of a cup anemometer and a vane positioned at 3.4 m above the ground. These instruments where connected to a Campbell CR1000 datalogger. At the HEES plot a HOBO Micro-Station was installed in a cleared area covered

by short ferns, with the temperature probe at 2 m, the solar radiation sensor and the wind speed and direction sensors at 3 m.

At both plots, precipitation was measured with Campbell ARG100 tipping bucket rain gauges, placed at 1 m above the vegetation. Following the methodology described by Calder and Kidd (1978), precipitation data were corrected for losses during bucket rotation using dynamic calibration at the laboratory. The relatively low wind speeds and the aerodynamic profile of the ARG100 rain gauge did not justify a correction for wind losses (Frumau et al., 2011). The two plots were located in sloping terrain with dominant winds trending perpendicular to the slope, the correction coefficient proposed by Sharon (1980) was applied following the procedure detailed by Ritter et al. (2008).

To compare the intensity of fog interception at the two sites, two identical cylindrical fog gauges (height 40 cm, 12 cm in diameter) made of a fine plastic mesh (1 mm) were placed at ca. 2 m above the ground in the clearings. Intercepted water was collected with a funnel at the base of the cylinder and diverted to a plastic container.

3.2. Throughfall and stemflow

Due to the existence of dripping points and shaded drier areas, the spatial variability of throughfall is usually high. To limit sampling error, an appropriate sampling scheme must be implemented (Staelens et al., 2006; Zimmermann et al., 2010). Throughfall was measured using two sampling designs (Domínguez González, 2011): (1) a continuous record from a set of troughs draining into a tipping bucket gauge, and (2) manually read small collectors (Holwerda et al., 2006b; Ziegler et al., 2009).

The troughs were made of 3m long PVC pipes of diameter 15 cm cut in half. To facilitate drainage, they were inclined at an angle greater than 15° from the horizontal. A set of 4 troughs were installed at the MESF plot (collection area of 1.8 m^2), while only 3 troughs could be fitted underneath the shrubs of the HEES plot (collection area of 1.3 m^2) (Fig. 3). Collected water was directed to a modified ARG100 10 cm^3 tipping bucket rain gauge. This instrumentation was calibrated in the field at a static rate with the following procedure. The troughs were initially wetted to avoid water storage. A precise amount of water was then dispersed over the troughs at a constant rate, and bucket tips were recorded until complete drainage. Water was poured at a rate of ca. 1 mm h^{-1}, which is close to the observed median rainfall rate, and sufficiently small to neglect losses from bucket rotation. For both plots, the amount of water measured by the tipping

bucket was ca. 10% smaller than the amount added. These losses were attributed to evaporation and splash from the tipping bucket, and could also be the consequence of a slight deviation of the tipping-bucket leveling. This correction factor derived from static field-calibration was applied to all throughfall data measured by the troughs. A correction derived from dynamic calibration of the ARG100 tipping bucket in the laboratory was applied, but given the weak intensity of throughfall during the period of investigation, this correction had only a negligible effect.

Water collected by the troughs was directed to a single automatic gauge, so that sampling error could not be inferred from these measurements. To this effect, small collectors were built from funnels 25 cm in diameter placed over 5-L containers. 33 collectors (total area of 1.6 m^2) were distributed randomly at the MESF plot while only 13 collectors (total area of 0.6 m^2) could be installed at the HEES plot (Domínguez González, 2011). The arrangement of these collectors remained fixed during the period of interest, measurements were performed manually, as far as possible after each precipitation events. Yet, difficulties of access to the field limited the number of readings.

Assuming throughfall spatial distribution to be random, relative sampling error expressed as percentage of the mean reads (e.g. Kimmins (1973); Thimonier (1998); Holwerda et al. (2006b)):

$$r_{se} = \frac{t_{\alpha,N-1} CV}{\sqrt{N}} \tag{1}$$

where $t_{\alpha,N-1}$ is the Student's t-value at the α level, N the number of collectors, and CV the coefficient of variation. Though throughfall collectors had different shapes (linear for troughs, and circular for small manual collectors), sampling total areas were similar for both collection methods, and sampling errors of trough measurements were inferred from r_{se} for the manual gauges. This is expected to overestimate trough sampling error since trough sampling area were somewhat larger than total collector area.

Stemflow was measured on each tree trunk within the MESF and HEES plots (26 and 12 trees, respectively). The stems were first cleaned of epiphytes and mosses in the area where the collecting spiral was to be installed. Stemflow collection was performed following a methodology similar to Crockford and Richardson (2000) and McJannet et al. (2007b). At 0.5-1.0 m above the ground, a split plastic hose (internal diameter 15 mm) was attached with staples to the stem following a spiral and then sealed with silicone. Containers of 2 L capacity were used to collect the water, and were

emptied after weighing using a portable electronic scale each two-three days. All the 26 tree trunks of the MESF plot, and all the 12 shrub stems of the HEES plot were instrumented. Although a few trees extended outside of the surface of the plot, this was most probably compensated by other trees with crowns overlapping the plot. Stemflow was converted to equivalent depth of water by dividing the total volume of water by the surface of the plot.

3.3. Interception model

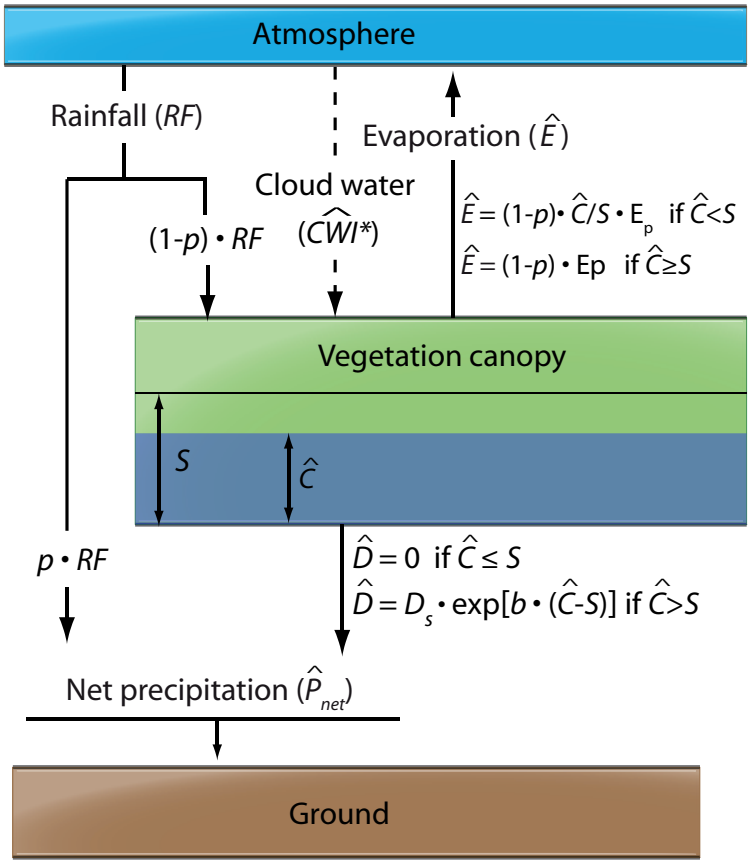

Figure 4: Schematic summary of the modified Rutter interception model (Rutter et al., 1972, 1975; Valente et al., 1997) with drainage function from Gash and Morton (1978).

Canopy evaporation and drainage were estimated with a modified *Rutter* model for interception losses (Rutter et al., 1972, 1975; Valente et al., 1997).

Contrary to the *Gash*-type models (Gash, 1979), *Rutter*-type models are based on a running water balance and do not require the separation of the period of interest into individual rainfall events (Muzylo et al., 2009). The interception model was implemented with the software R (R Development Core Team, 2009).

All variables referring to a water storage, or flux, were expressed as depth of water over the whole plot area. For each time step, the canopy water storage $\hat{C}$ is recharged by the amount of rainfall (RF) intercepted by the canopy, $(1-p) \times RF$, where p is the free throughfall coefficient. The input from fog interception, which remains unknown at this point is not considered yet. Given the small amount of water diverted by stemflow in our study plots and the difficulties to implement a constant monitoring, the separated compartments for trunk water storage and evaporation introduced by Rutter et al. (1975) and Valente et al. (1997) were not included in this model. Estimates of canopy drainage ($\hat{D}$) included both throughfall and stemflow. An exponential function was used to calculate drainage from the canopy (Gash and Morton, 1978; Schellekens et al., 1999):

$$\hat{D} = \begin{cases} D_s \times \exp[b(\hat{C} - S)] & \text{if} \quad \hat{C} > S \\ 0 & \text{if} \quad \hat{C} \leq S \end{cases} \tag{2}$$

where parameters S [mm], D_s [mm h^{-1}] and b [mm^{-1}] are characteristic for the canopy. S is the amount of water stored by the canopy that will not drip to the ground, defined as *adherent storage capacity* by Liu (2001). Adherent storage is opposed to transient storage, the amount of water temporarily stored by the canopy which finally drips to the ground. In accordance with these definitions, drainage is set to zero when $\hat{C} \leq S$ (Gash and Morton, 1978; Schellekens et al., 1999).

The estimate of evaporation from the canopy was obtained following the scheme of the *sparse* version of the *Rutter* model (Valente et al., 1997). In this version, only evaporation from the canopy cover is considered and any understorey evaporation is neglected. When the canopy is saturated ($\hat{C} \geq S$), estimated actual evaporation ($\hat{E}$) reaches potential evaporation, $\hat{E} = (1-p) \times E_p$. For unsaturated canopy ($\hat{C} < S$), $\hat{E}$ is considered to be proportional to the canopy saturation ratio $\hat{C}/S$, which reads (Klaassen, 2001; Rutter et al., 1975; Valente et al., 1997):

$$\hat{E} = \begin{cases} (1-p) \times E_p & \text{if} \quad \hat{C} \geq S \\ (1-p) \times \hat{C}/S \times E_p & \text{if} \quad \hat{C} < S \end{cases} \tag{3}$$

where E_p was estimated with the Penman-Monteith (P-M) equation with the surface resistance set to zero (Monteith, 1965). Net long-wave radiation was not considered in the calculation, which is a common assumption in the context of dense fog (Holwerda et al., 2010a; Muñoz-Villers et al., 2011; Wallace and McJannet, 2006). For moderate wind speeds, aerodynamic resistance r_a of wet vegetation may be estimated from Rutter et al. (1972, 1975):

$$r_a = \frac{1}{k^2 u_z} \cdot \left(\ln \left(\frac{z-d}{z_0} \right) \right)^2 \tag{4}$$

where $k = 0.4$ is the von Karman constant, u_z is wind speed and z its measurement height. z_0 is the roughness length and d the zero plane displacement. For both stands, it was assumed that $d = 0.75 \cdot h$ and $z_0 = 0.1 \cdot h$, which are the values stated by Rutter et al. (1975) for leafy vegetation. Temperature, relative humidity and wind speed measured at the weather station in the clearings were assumed to be representative of the conditions at 2 m above the instrumented canopy. Pearce et al. (1980) showed that this assumption could induce an overestimation of potential evaporation, but this effect will be supposed to be of limited effect in the present study, since canopy heights were relatively small and meteorological variables were taken close to the forested plots. Values of relative humidity were not available at the HEES plot (cloud center), values from the MESF plot (cloud base) were used for the calculations. This is not expected to induce a significant overestimation of evaporation at the HEES plot, since relative humidity at the MESF plot was often at, or close to 100%. Given these assumptions, the estimation of r_a may be inaccurate but the estimation of potential evaporation should remain relatively fair, since the radiative term is expected to dominate evaporation from a wet canopy in contexts of small vapor pressure deficit and limited wind speeds (Klaassen, 2001; Holwerda et al., 2010a).

A schematic summary of the canopy water budget model is presented in Fig. 4. In the absence of cloud water interception, the wet canopy water budget equation can be written as follows:

$$RF = \hat{P}_{net} + \hat{E} + \Delta\hat{C} \tag{5}$$

where net precipitation $\hat{P}_{net}$ reads:

$$\hat{P}_{net} = (p \times RF) + \hat{D} \tag{6}$$

Canopy parameters p, S, have been estimated from a carefully chosen set of rainfall events. These events had to be compatible with the

definition given by Gash (1979): a fully dry canopy at the beginning of the event, rainfall at a constant rate, and termination of the event at the end of dripping from the canopy. Furthermore, it was essential to select events where cloud interception was negligible. We therefore selected events with the lowest (TF/RF) ratios, where TF is measured throughfall. The *within-event analysis* detailed by Link et al. (2004) was implemented. The principles are relatively straightforward: at the beginning of an event, the canopy is dry and net precipitation is limited to the fraction of rain passing through canopy gaps. If we neglect evaporation during rainfall, we can write $P_{net,cum} = p \times RF_{cum}$ where $P_{net,cum}$ is cumulative net precipitation and RF_{cum} is cumulative rainfall. Once the canopy is saturated ($\hat{C} = S$), net precipitation rate becomes close to the rainfall rate. The cumulative curve of net precipitation becomes steeper and we can write $P_{net,cum} = -S + RF_{cum}$. Considering the plot of cumulative net precipitation against cumulative gross precipitations, the parameters p and S can be estimated from two linear regressions. Parameter p is the slope of the first regression line before the slope break (before saturation of the canopy). Like Takahashi et al. (2011), S was inferred from the x-intercept of the second regression line, after the slope break (i.e. once the canopy is saturated).

The parameters D_s and b were estimated by non-linear least square optimization of the RMSE between modeled net precipitation ($\hat{P}_{net} = \hat{D} + (p \times RF)$) and observed net precipitation (P_{net}) at a 15-min time step.

Given the limited variability of canopy structure in this study, the interception model parameters characterizing the canopy (p, S, D_s, b) have been considered constant throughout the investigation period.

3.4. Cloud water interception

The interception model is first run considering only rainfall as input (Eq. 5). The initial estimate of cloud water interception ($\widehat{CWI}_0$) is deduced as follows:

$$\widehat{CWI}_0 = P_{net} - \hat{P}_{net,1} \tag{7}$$

where P_{net} is observed net precipitation and $\hat{P}_{net,1}$ is the predicted value after the first run of the interception model. The term $\widehat{CWI}_0$ explains the difference between measured net precipitation (P_{net}) affected by CWI and the predicted value ($\hat{P}_{net,1}$), where CWI has been disregarded (Holwerda et al., 2010a; McJannet et al., 2007b; Takahashi et al., 2011). Considered

over the whole period of interest, the water budget considering measured net precipitation reads:

$$RF_{cum} + \widehat{CWI}_{0,cum} = P_{net,cum} + \hat{E}_{1,cum} \tag{8}$$

where RF_{cum} and $P_{net,cum}$ are measured cumulative rainfall and net precipitation, respectively, while $\widehat{CWI}_{0,cum}$ and $\hat{E}_{1,cum}$ are the first estimates of cumulative CWI and evaporation, respectively.

If CWI is negligible, $\widehat{CWI}_{0,cum}$ should be around zero over the period of interest. With CWI occurrence, $\widehat{CWI}_{0,cum}$ should be clearly positive. Yet, any time lag between rainfall and throughfall may cause $\widehat{CWI}_0$ values to be underestimated or even to become negative, which is not realistic. In order to reduce the occurrence of negative values, the time series is smoothed with a 1.75 h (7×15 min) moving average filter (Takahashi et al., 2011). Unless the evaporation estimate is inaccurate, the remaining negative values should then be in limited numbers and are set to zero. The smoothed, corrected estimate of CWI is written $\widehat{CWI}_0^*$. Setting negative values to zero introduces an error in the water balance (Eq. 8). The estimate of CWI is therefore adjusted:

$$\widehat{CWI}_1^* = k_1 \times \widehat{CWI}_0^* \tag{9}$$

where k_1 reads:

$$k_1 = \frac{\left(P_{net,cum} + \hat{E}_{1,cum} - RF_{cum}\right)}{\widehat{CWI}_{0,cum}^*} \tag{10}$$

When the input from CWI is significant, the estimate of evaporation from the first run ($\hat{E}_1$) may underestimate actual evaporation (Takahashi et al., 2011). An iterative approach is then implemented to improve the estimates of evaporation and CWI. For $i \geq 2$, both measured rainfall (RF) and estimated fog interception ($\widehat{CWI}_{i-1}^*$) are considered for the calculation of canopy water storage ($\hat{C}_i$). The interception model water budget (Eq. 5) is therefore modified:

$$RF + \widehat{CWI}_{i-1}^* = \hat{P}_{net,i} + \hat{E}_i + \Delta\hat{C}_i \tag{11}$$

where $i \geq 2$ is the model run number, and $\hat{P}_{net,i}$, $\hat{E}_i$ and $\hat{C}_i$, are the corresponding estimates of net precipitation, evaporation, and canopy water storage, respectively. After each run of the interception model, the estimate of CWI is updated from a generalization of Eqs. 9 and 10 with:

$$k_i = \frac{\left(P_{net,cum} + \hat{E}_{i,cum} - RF_{cum}\right)}{\widehat{CWI}^*_{i-1,cum}} \tag{12}$$

The adjustment factor k_i should becomes close to one after a certain number of runs (say $i = n$). Further runs of the interception model don't change significantly the estimate of CWI, which can be considered as satisfactory. The finalized estimate of cloud water interception, $\widehat{CWI}^*_n$ is written $\widehat{CWI}^*$.

The error of CWI depends on measurement and sampling errors for rainfall, stemflow, throughfall, temperature, solar radiation, wind speed, and relative humidity. Furthermore, it depends on the validity of the assumptions and the choice of the parameters used for the interception model. In a first attempt to characterize the error on CWI, only the sampling error on net precipitation and the calibration error of the interception model are considered. Assuming both errors to be independent, the total uncertainty of $\widehat{CWI}^*$ reads:

$$\epsilon(\widehat{CWI}^*) = \sqrt{\epsilon(P_{net})^2 + \epsilon(\hat{P}_{net})^2} \tag{13}$$

where the error of measured net precipitation is restricted to the throughfall sampling error (Eq. 1), $\epsilon(P_{net})^2 = r_{se} \cdot TF$, where TF is measured throughfall. The error in modeled net precipitation is estimated from the RMSE of the calibration dataset, $\epsilon(\hat{P}_{net})^2 = n \cdot (RMSE)^2$ where n is the number of 15-min estimates.

4. Results

4.1. Climatic conditions

The 2010 *garúa* fog season extended from end of June to December and was characterized by low temperatures and weak continuous rainfalls (Fig. 5 A). With respect to long term conditions recorded at station CDF2 (1987-2010), precipitation remained close to the median in 2010 but temperatures were lower due to the *La Niña* anomaly (National Weather Service Climate Prediction Center, 2011) (Fig. 5 B).

The MESF station was operational from July 2010 onwards, but due to difficulties with setting up the HEES station, simultaneous records were only available from September 2010 onwards. Very humid conditions together with difficulty of access made the acquisition of continuous records challenging. Yet, seventy-five days with complete, quality-checked data for

the two stations were obtained. Given the relatively stable climatic conditions during the *garúa* season, the current dataset can be considered as being representative for the whole 2010 *garúa* season.

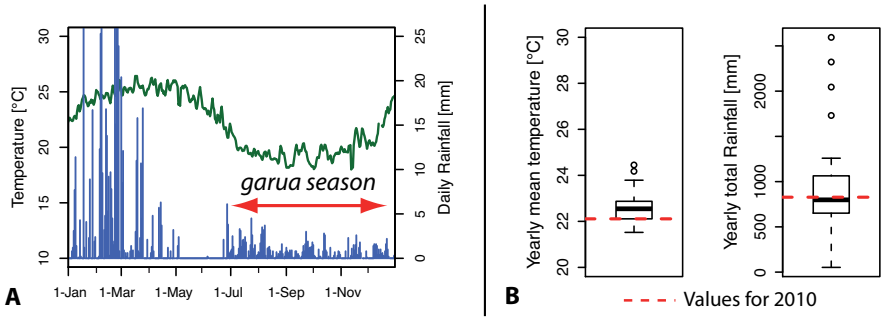

Figure 5: (A) Temperature and rainfall recorded at station CDF2 (Alt. 180 m a.s.l.) in 2010. Low temperatures and continuous low-intensity rainfalls characterize the *garúa* season (red arrow). (B) 2010 context compared to 1985-2010 long-term records. It was a relatively cooler year due to the *La Niña* anomaly (left), while total rainfall remained close to the annual median (right).

Air temperature at the MESF station was 17.5 °C on average, which is 2 °C higher than at the HEES station. Solar radiation was comparable at the two stations, and remained low throughout the season (daily average close to 100 W m^{-2}). Due to the observed dense cloud cover, median relative short wave radiation was close to 30% of theoretical clear-sky radiation. As may be expected in these conditions, relative humidity was for much of the time at or close to 100% at the MESF plot. Though not measured at the HEES plot, relative humidity could only be higher there due to more frequent fog occurrence. Wind speed was relatively weak at the MESF station, with a mean of 0.9 m s^{-1}. Wind speed was significantly higher at the HEES plot, with a mean of 2 m s^{-1}. Rainfall records at stations CDF2, MESF and HEES highlight the marked orographic effect (Fig. 6). During simultaneous monitoring at both stations (75 days), total rainfall was 238 mm at the MESF station, and 313 mm at HEES station (28% higher). Median precipitation rates were small at both of the stations, 0.8 mm h^{-1} and 1.1 mm h^{-1} respectively. Daily rainfall totals at the two stations were highly correlated ($RF_{HEES} = 1.11 \cdot RF_{MESF} + 0.34$, with $r^2 = 0.89$ and $n = 104$). This allowed the filling of short data gaps (of a few days).

Water collected by fog gauges could not be recorded continuously and may therefore not be fully representative of the whole period of interest.

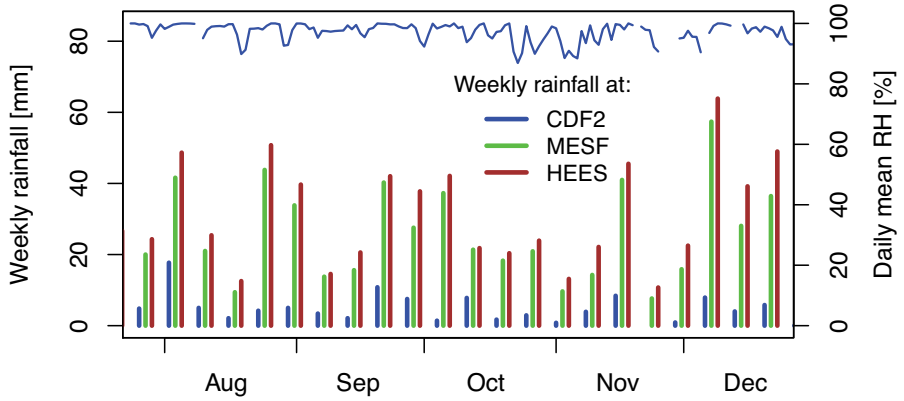

Figure 6: Weekly rainfall records for CDF2, MESF and HEES stations during the 2010 *garúa* fog season highlight the marked orographic effect. Mean daily relative humidity at the MESF station remained close to saturation.

Yet, during a simultaneous recording period of 15 days, water collected by the fog gauges at the HEES plot was 5 times higher than at the MESF plot. During this recording period, rainfall total at the uppermost HEES station was only 25% higher than at the MESF station. The marked difference in catch by the fog gauges is interpreted by denser and more frequent fog blown by faster winds at the HEES station, which is compatible with field observations.

4.2. Throughfall and stemflow

Coefficients of spatial variation of throughfall (CV) inferred from the manually read collectors were similar for both plots, ranging between 40% and 60% with a mean of 50%. This latter value was used to estimate the sampling error for the troughs (assumed to be constant). The corresponding sampling error at the 68% confidence level (Eq. 1) was 8.8% for the MESF plot and 13.9% for the HEES plot. Due to the clogging of the throughfall tipping buckets and issues with the instrumentation, throughfall data was unavailable during 10% and 22% of the period of interest (September-December), for MESF and HEES plot respectively. Throughfall collected during the seventy-five days of simultaneous monitoring was 188 ±15 mm at the MESF plot, and 360 ±50 mm, at the HEES plot. This corresponds respectively to 79 ±8% and 115 ±16% of incident rainfall.

During the period of stemflow collection (40 and 31 consecutive days, respectively, at MESF and HEES plots), the amount of stemflow collected was 0.7% of incident rainfall (0.8% of throughfall) at the MESF plot, and 0.6% of incident rainfall (0.5% of throughfall) at the HEES plot. High proportions of stemflow are often associated with high rainfall rates (Bruijnzeel et al., 2011). The small amount of stemflow collected in the present study may therefore be explained by the low rainfall rates observed during the *garúa* season. Epiphytes were present at the two sites, when they are partly unsaturated between rainfall events, they may store subsequent water inputs and reduce stemflow (Hölscher et al., 2004; Köhler et al., 2007). Furthermore, some specific characteristics of the vegetation participate to the diversion of stemflow to throughfall (Crockford and Richardson, 2000): leaning trunks, sub-horizontal branches, flow path obstructions such as detaching bark peaces, apex of the leaves orientated to the ground. These features were especially represented at the MESF plot.

Given the small amount of water diverted to stemflow, it was not continuously recorded. For the estimation of CWI (Eq. 7), net precipitation ($P_{net} = TF + SF$) was calculated at the 15-min time step from throughfall data multiplied by a constant correction factor (1.008 at MESF plot, 1.005 at HEES plot).

4.3. Interception model

Canopy characteristics for the interception model are detailed in Table 2. Free throughfall coefficient p and canopy storage capacity S were estimated from rainfall events with the low relative throughfall (TF/RF), i.e. with negligible fog interception. Due to the rapid saturation of the canopy (Fig. 7), the relatively coarse resolution of the tipping bucket rain gauge (0.2 mm) was a limitation for an accurate estimation of p.

	MESF	HESS
p [$-$]	0.20	0.30
S [mm]	0.56	0.23
D_s [mm h^{-1}]	0.20	0.25
b [mm^{-1}]	1.99	1.72

Table 2: Canopy characteristics as used in the modified *Rutter* model. Free throughfall coefficient (p) and water storage at saturation (S) were estimated by linear regression. Drainage function parameters D_s and b were estimated by non-linear least square optimization.

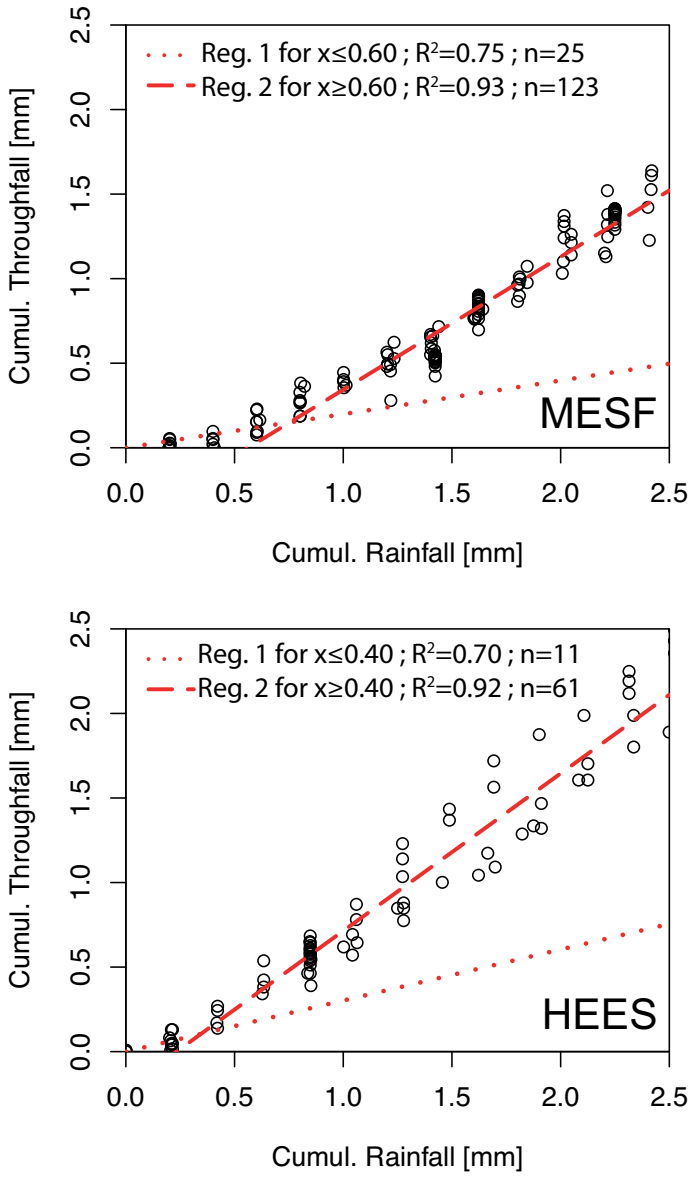

Figure 7: Estimation of canopy characteristics p and S with the *within-event* analysis for the MESF (top) and HEES (bottom) plots.

Free throughfall coefficients estimated by the graphical method ($p = 0.20$ and $p = 0.30$, respectively, for MESF and HEES plots) were comparable to the values of canopy gap fraction estimated from vertical photographs (0.30 and 0.26, respectively, for MESF and HEES plots) (Table 1). Nevertheless, gap fraction values estimated from photographs are not as appropriate in the sense that the view angle is not strictly vertical, particularly on the edges of the photographs. The graphical method will be preferred, since it is devoid of such edge effect, and takes into account the actual angle of incidence of rainfall as it reaches the canopy.

D_s and b were obtained by least square optimization of predicted net precipitation ($\hat{P}_{net}$) against observed values (P_{net}) during the same events with low relative throughfall at 15 min time step. The RMSE of 15 min estimates in the calibration dataset was 0.04 mm for the MESF plot and 0.06 mm for the HEES plot. Predicted net precipitation was overestimated by 11.2% and 2.1%, respectively, for MESF and HEES plots. This reflects an under-estimation of E by the P-M equation during calibration events.

4.4. Fog interception

During the period of simultaneous records at both of the stations (75 days, extending from September to December 2010), cumulative $\widehat{CWI}_0$ at the MESF plot was slightly below zero (-10 mm). This negative value is the consequence of the slight bias highlighted during the optimization of D_s and b, and may conceal short periods with effective CWI. Yet, this finding indicates that CWI at the MESF plot was only a very minor input, and it was therefore neglected. In contrast, cumulative $\widehat{CWI}_0$ was 73 mm at the HEES plot, which reflects a significant input from CWI. The smoothed, corrected, and adjusted estimate $\widehat{CWI}_1^* = k_1 \times \widehat{CWI}_0$ was therefore computed ($k_1 = 0.88$) and used for a second run of the model. With $k_2 = 1.10$, it was necessary to run the model a third time, which yielded $k_3 = 1.006$. Cumulative evaporation increased by 30% between the first and the third run of the model ($E_{1,cum} = 27$ mm, $E_{2,cum} = 34.5$ mm, $E_{3,cum} = 35$ mm). The finalized estimate $\widehat{CWI}^*$ was 81 ± 50 mm at the HEES plot, representing 26 $\pm$16% of incident rainfall (RF), or 20 $\pm$13% of all water inputs ($RF + \widehat{CWI}^*$). The daily interception rate was in average 1.18 mm day^{-1} and reached 5.24 mm day^{-1} at the maximum.

The effect of wind speed on fog catch was investigated from the 15-min estimates of CWI at the HEES plot (Fig. 8). As depicted in Fig. 9, the variability of $\widehat{CWI}^*$ increases markedly with wind speed. Median $\widehat{CWI}^*$ is

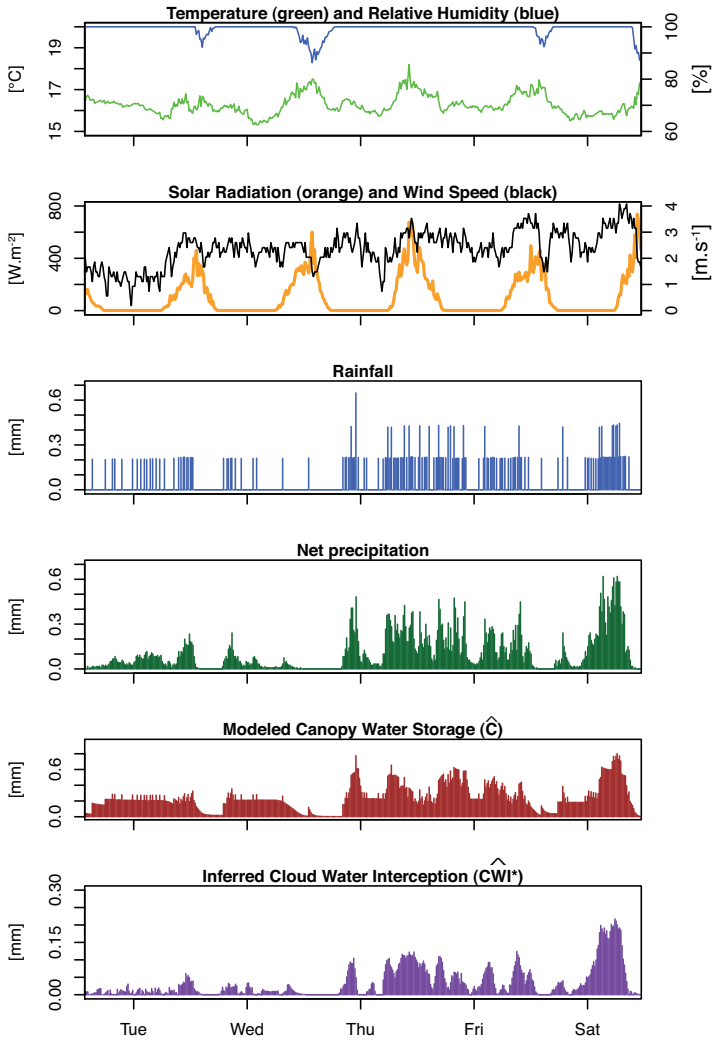

Figure 8: Climatic variables and modeled canopy water storage $\hat{C}$ and $\widehat{CWI}^*$ estimates for the HEES station between 15 and 20 November 2010, with 15-min time steps.

ca. 0.03 mm h^{-1} for wind speed between 0 and 2 m s^{-1}, while it reaches 0.06 mm h^{-1} for wind speed higher than 2 m s^{-1}. $\widehat{CWI}^*$ rates for wind speed intervals [2;3] and [3;4] m s^{-1} were significantly greater than for wind speed intervals [1;2], and [2;3] m s^{-1}, respectively (Wilcoxon rank sum test, $p < 0.01$ for both of the pairs). Such a pattern was not identified for other recorded parameters (temperature, solar radiation, relative humidity).

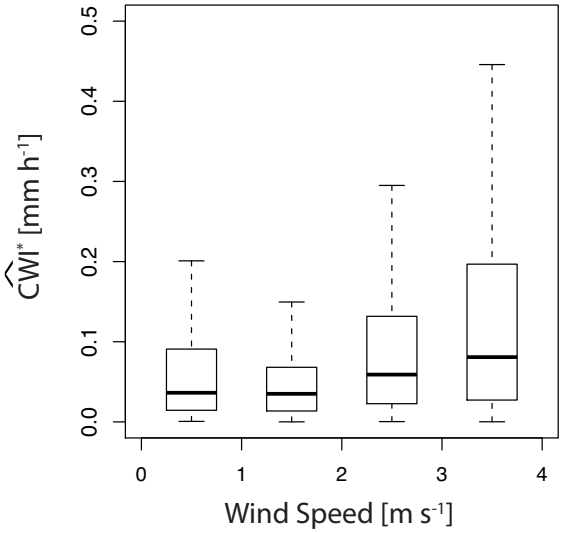

Figure 9: Statistics of cloud water interception rates ($\widehat{CWI}^*$) classified for four wind speed intervals at the HEES plot. For higher wind speeds, *CWI* rates are higher and more scattered. Wind speed enhances *CWI* but is not the only controlling factor.

These results highlight the positive influence of wind speed over *CWI*, but the scatter of *CWI* rates for higher wind speeds demonstrates the existence of other controlling parameters, such as fog liquid water content (*LWC*).

5. Discussion

5.1. Interception model

Gash-type models require the separation of the period of interest into individual precipitation events as defined by Gash (1979), namely continuous rainfall and evaporation rates, as well as a dry canopy at the beginning and

termination of the event. Given these restrictive conditions, event separation can be challenging and subjective (Llorens et al., 1997; Llorens, 1997). This is particularly true in the context of fog occurrence, with continuous rainfall, weak evaporation rates, and the vegetation canopy remaining wet. The modified *Rutter* model used in this study is based on a running canopy water budget and avoids such event separation over the whole period of interest. The selection of a set of events is yet required for the estimate of model parameters. The introduction of the drainage function proposed by Gash and Morton (1978) provided a more accurate estimation of net precipitation for shorter time steps.

The sensitivity of *Rutter* models to parameters p and S has been investigated by Valente et al. (1997) and Gash and Morton (1978). Uncertainty for these parameters was relatively high in this study, which can be attributed to parameter variability from event to event (Jackson, 1975; Link et al., 2004; Massman, 1983), a slight incompatibility with the Gash (1979) conditions for sample storms, evaporation from the canopy during rainfall (Link et al., 2004), and the resolution of the rain gauge (0.2 mm), being to coarse with respect to event size and canopy storage capacity.

Free throughfall coefficients obtained for MESF and HEES plots ($p = 0.20$ and $p = 0.30$, respectively) are within the common range reported in the literature (e.g. Holwerda et al. (2006a), Takahashi et al. (2011), García-Santos (2007), and Návar and Bryan (1994)). The value of canopy storage capacity found for the secondary forest of the MESF plot ($S = 0.56$ mm) is similar to the value estimated by Holwerda et al. (2006a) for a plot of 3 m high, evergreen forest in Puerto Rico ($S = 0.5$ mm). Nevertheless, higher values were generally attributed to medium-sized tropical forests: 0.85 mm for a plot of 12.5 m high guava trees in Hawaii (Takahashi et al., 2011), between 1.08 and 1.23 mm for 9-13 m high laurel and mixed-tree heath/beach forests in the Canary Islands (García-Santos, 2007), and 1.3 mm for a 5-8 m high tropical forest in Jamaica (Hafkenscheid et al., 2002). The value of S found for the endemic shrubs of the HEES plot (0.23 mm) is particularly small, but comparable to the values of 0.29 mm found for 4 m high shrubs in Spain (Domingo et al., 1998). Návar and Bryan (1994) found higher values, ranging between 0.39 and 1.59 mm for 1.8-2.2 m semi-arid, dense scrub vegetation in Mexico. Apart from measurement errors, relatively common values for p associated with small values for S can be attributed to the single storey tree architecture, and the very sparse understorey vegetation observed at the two plots.

While the accuracy of net precipitation measurements can be assessed and even reduced by the use of an adapted sampling strategy (Holwerda et al., 2006b; Ziegler et al., 2009; Zimmermann et al., 2010), the uncertainties of evaporation estimates are difficult to overcome. On the calibration dataset, predicted net precipitation was overestimated by 11% and 2%, respectively, for MESF and HEES plots, which can be explained by an underestimation of evaporation. Other observations can be interpreted in terms of a slightly underestimated evaporation. In particular, some nightly rainfall events at the MESF plot presented relative throughfall (TF/RF) smaller than 100%, while the P-M equation predicted zero evaporation. The accuracy of potential evaporation estimates may be affected by measurement errors and the occurrence of processes that are not taken into account in the P-M equation. Relative humidity was measured by a probe within a protection shield, which can remain soaked after a prolonged humid period, while the outside becomes drier. This issue has been highlighted by Frumau et al. (2006) and Holwerda et al. (2006a, 2010a) and may be addressed with dry- and wet-bulb temperature monitoring. The underestimation of potential evaporation could as well be explained by an overestimation of the aerodynamic resistance (r_a). Holwerda et al. (2012) showed that in areas with complex topography, r_a could be overestimated, which induces an underestimation of E_p.

Various studies have highlighted an underestimation of evaporation with the P-M equation without apparent errors from the instrumentation. They invoke processes such as the condensation of water vapor above the vegetation canopy (Scatena, 1990; Schellekens et al., 1999, 2000) or the effect of advection from the nearby ocean (Dykes, 1997; Holwerda et al., 2006b; McJannet et al., 2007a; Schellekens et al., 1999, 2000). With the occurrence of orographic rainfall and the proximity to the Pacific Ocean, both of these processes can be expected along the windward slope of Santa Cruz, but their actual significance is challenging to quantify.

The choice of the time step is critical for the interception model. Shorter time steps allow the investigation of processes related to meteorological parameters changing at small time scales such as wind speed, and improve the estimate of potential evaporation. Yet, various limitations regarding the instrumentation and the interception model prevent the use of short time steps. Tipping bucket gauges do not allow high-frequency precipitation monitoring for small precipitation rates. The device resolution (precipitation height per bucket rotation) is a limiting factor. A reduction of the

bucket size is possible, but introduces measurement errors for higher precipitation rates (Calder and Kidd, 1978). Also, it becomes challenging to predict canopy drainage at higher frequency. Canopy dripping may not be continuous but rather depend on wind gusts and other parameters which are not taken into account in the interception model. Given the instrumentation and context of this study, it appeared challenging and of limited interest to predict fog interception for time steps shorter than 15 min.

5.2. Cloud water interception

Cloud water interception (CWI) was negligible at the MESF plot, significant at the HEES plot. The average daily CWI rate found for the HEES plot during the 2010 *garúa* season (1.18 mm day^{-1}) is comparable to other low-elevation elfin cloud forests under low precipitation: 0.43 mm day^{-1} for low shrubs and trees on the leeward side of Maui (Hawaii) (Giambelluca et al., 2011), 0.85 mm day^{-1} and 2.35 mm day^{-1} in Colombia at low and high elevation respectively (Cavelier and Goldstein, 1989). Studies reviewed by Bruijnzeel et al. (2011) report CWI contributions ranging between 4% and 45% with a mean of 16% of incident rainfall. This places the current estimate of CWI for the HEES plot (26% $\pm$ 16% of incident rainfall) in the upper central range of other studies, similar to Holwerda et al. (2006a); Hutley et al. (1997); McJannet et al. (2007c). Such a comparative analysis of CWI rates would be more relevant if the same methodology was employed for each of the study sites, which is not the case here.

Short time steps allowed the investigation of the correlation between wind speed and CWI rates. Mean CWI rate increases with higher wind speed (Fig. 9). This can be explained by a higher impaction rate of wind-driven fog droplets against leaves and branches. The scatter of CWI for higher values of wind speed highlights the effect of other controlling parameters, such as fog liquid water content (LWC) which could not be measured in the field. Eugster et al. (2006) showed that net cloud water flux increases with higher LWC. The combined effects of wind speed and LWC over CWI rates have been discussed by Villegas et al. (2008). They state that optimum conditions for CWI are found for medium values of liquid water content and wind speed. For higher wind speeds, it is expected that an increase in potential evaporation reduces effective CWI. This effect is not visible in the current dataset. Either wind speed, or air vapor pressure deficit remained too low for such an effect to become effective. Furthermore, it should be noted that an increase in fog droplet interception by the canopy

is not the only process that can be invoked to explain the rise in net precipitation for higher wind speeds. Indeed, this may also be attributed to the sudden dripping caused by wind gusts. In fact, both processes probably act simultaneously. Defining their respective contributions appears challenging, if not impossible.

In a first attempt to characterise the uncertainty of *CWI*, the errors of measured and predicted net precipitation were added quadratically (Eq. 13). Similarly to other studies, the uncertainty of *CWI* was high due to the propagation of errors from both sampling and modeling. The term related to throughfall sampling error dominates, but is expected to be an overestimation. Indeed, trough sampling error was estimated from the set of manual collectors, with a smaller total collection area. Instead of implementing uncertain corrections, it was preferred to keep the latter error estimate, which is safer considering that throughfall was assumed to have a random spatial distribution and a constant coefficient of variation, and that other potential sources of error were disregarded.

5.3. Comparative analysis of the two study sites

Wet canopy water budgets for the two study sites are shown to be very contrasting (Fig. 10). At the MESF plot, net precipitation under the secondary forest represented 79 ± 8% of incident rainfall and *CWI* was found to be negligible. At the HEES plot (2 km further north and situated 150 m higher), net precipitation was two times higher. This difference is explained by the contribution of *CWI*, higher rainfall (+31%), and lower evaporation (-21%).

As illustrated by Fig. 9, higher wind speed is related to higher *CWI* rates. Yet, the difference in mean wind speed at the MESF and HEES stations (respectively 0.9 m s^{-1} vs. 1.9 m s^{-1}) alone can not explain the observed difference in fog catch. The contrast between the two study sites most probably originates from the combined effects of higher wind speeds, better exposure to dominant winds, and more frequent, denser fog at the HEES station. The latter is confirmed by the higher water catch by the fog gauge at the HEES station, which was five times higher than at the MESF station. With steeper slopes and discontinuous shrub patches varying in height, the endemic *Miconia* shrubs of the very humid zone are better exposed to the dominant winds than the large patches of secondary forest on flatter terrain.

The higher storage capacity and lower free throughfall coefficient of the secondary forest (MESF plot) may partly explain that evaporation was

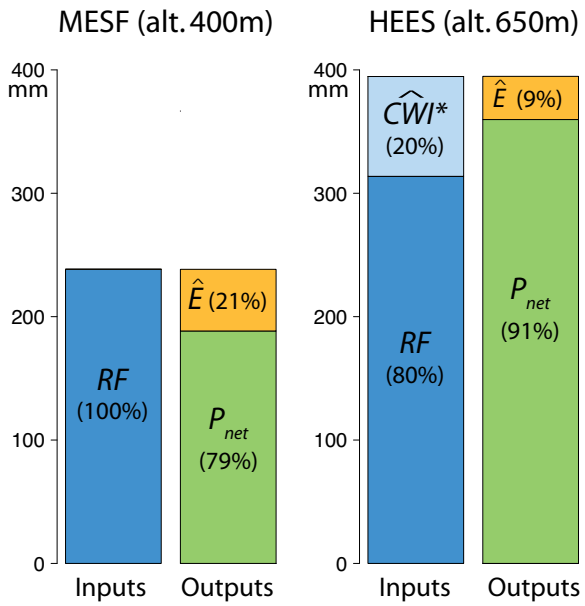

Figure 10: Canopy water budget at the MESF plot (left) and the HEES plot (right) for the seventy-five days of common monitoring. Inputs considered are corrected rainfall (RF) and cloud water interception ($\widehat{CWI}^*$). $\widehat{CWI}^*$ was not significant at the MESF plot, while it represented 20% of water inputs at the HEES plot.

higher at the MESF site. However, it is difficult to conclude on the role played by canopy structure with such contrasting climatic conditions between the two sites. Within the framework of future studies, it would be interesting to compare *CWI* under other species present in the very humid zone (e.g. *Cinchona pubescens*).

Secondary forests cover about one third of the agricultural humid zone of Santa Cruz Island. The MESF plot was chosen as it was thought to be sufficiently representative, but some heterogeneities in the species distribution may induce different interception rates (e.g. Takahashi et al. (2011)). Extending the results of the MESF plot to all forest patches of the agricultural humid zone may be hazardous. Additional plots would be needed to ascertain the associated variability in net precipitation.

The HEES plot is considered representative of a significant part of the high-elevation very humid zone (Fig. 2). Though the invasive *Cinchona pubescens* tree is still present in the very humid zone, it is the object of a control program by the *Galapagos National Park* so that the endemic *Miconia robinsoniana* shrub (included in this study) is expected to become more representative.

In the very humid zone, soils are thin and have a limited retention capacity, whereas atmospheric transpiration demand is very low. Runoff rapidly flows into open fractures and does not reach the agricultural zone below. Like in the Canary islands (García-Santos, 2007), groundwater recharge is enhanced in such a context. The very humid zone of Santa Cruz is likely to be of major importance for the groundwater resources of the island.

6. Summary and conclusions

The estimation of *CWI* was performed with the wet canopy water budget method, based on a *Rutter*-type interception model. This methodology presents the following characteristics:

- The *Rutter*-type interception model avoids the time-consuming, subjective separation of the whole period of interest into individual rainfall events.

- Canopy parameters p and S are estimated with the methodology detailed by Link et al. (2004) from a set of selected events fitting the conditions for sample storms defined by Gash (1979), and with negligible effect from *CWI*. From this same set of events, parameters of the

drainage function (D_s and b) are estimated by non-linear least square optimization.

- *CWI* is estimated for short time steps (15 min) as the difference between predicted and measured net precipitation. This allows the investigation of controlling factors varying in the short term, mostly wind speed. When *CWI* is significant, an iterative approach is implemented to take into account the input from fog on the estimate of evaporation.

It would be of the highest interest to compare this methodology with others at the same site, and to compare different sites with this methodology.

The results of this study highlighted the contrasting hydrological conditions along the windward slope of Santa Cruz Island during the fog *garúa* season:

- At the lower fringe of the cloud, in the secondary forest (MESF station, alt. 400 m a.s.l.), relative throughfall was 79% of incident rainfall. Fog interception was negligible.

- Only 2 km further north, in the center of the cloud belt, underneath the endemic *Miconia* shrubs (HEES station, alt. 650 m a.s.l.), relative throughfall was 115 ± 16% of incident rainfall. This was explained by the added input from *CWI*, which was estimated at 26 ± 16% of incident rainfall.

- Observed evaporation rates were locally higher than predicted with the P-M equation. This was interpreted as being due to difficulties with the measurement of relative humidity, the possible overestimation of aerodynamic conductance, and the effect of other sources of energy (latent heat released by condensation, advected air from the nearby ocean). As a consequence, *CWI* was to some extent underestimated.

- At the HEES plot, median *CWI* rate for wind speeds ≤ 2 m s^{-1} was ca. 50% lower (0.03 mm h^{-1}) than for wind speeds ≥ 2 m s^{-1} (0.06 mm h^{-1}).

Due to a significant input from *CWI*, higher rainfall and smaller evaporation, net precipitation underneath the endemic shrubs of the very humid

zone was two times higher. Given the high infiltration capacity and the limited transpiration expected in this zone, this additional input of water directly contributes to groundwater recharge. The very humid zone has therefore a significant role in the hydrology of the island and is sensitive to fog occurrence. Should climate change induce a raise of the cloud base or a reduction of fog occurrence, it would most probably induce a significant reduction of net precipitation, and therefore groundwater recharge in the very humid zone.

7. Acknowledgments

This study has been performed in the frame of the project *Galapagos Islands Integrated Water Studies* (GIIWS), funded by the Agence Nationale de la Recherche (ANR-blanc 2010 GIIWS Ref. 601-01). The GIIWS team would like to thank its local partners in the Galapagos: the Charles Darwin Research Station, the Galapagos National Park, and private land owners who allowed the installation of weather stations. Marta González del Tánago (Polytechnic University of Madrid) provided valuable advices for the set up of stemflow collectors. The authors are very grateful to Mandy Trueman (Charles Darwin Foundation & University of Western Australia), Heinke Jäger (Department of Ecology, Technische Universität Berlin), Anne Guézou (Charles Darwin Foundation), Julien Tournebize (Cemagref Antony) and Jean-Paul Lhomme (LISAH Montpellier) for their support on the field and corrections on the draft. Finally, the helpful comments by Prof. L.A. Bruijnzeel and another anonymous reviewer are gratefully acknowledged.

8. References

Brauman, K.A., Freyberg, D.L., Daily, G.C., 2010. Forest structure influences on rainfall partitioning and cloud interception: A comparison of native forest sites in Kona, Hawai'i. Agr. Forest Meteorol. 150, 265 – 275.

Bruijnzeel, L.A., 2001. Hydrology of tropical montane cloud forests: a reassessment. Land Use and Water Resources Research 1, 1–18.

Bruijnzeel, L.A., Burkard, R., Carvajal, A., Frumau, A., Köhler, L., Mulligan, M., Schellekens, J., Schmid, S., Tobón, C., 2006. Final Technical Report DFID-FRP Project no. R7991. Hydrological impacts of converting tropical montane cloud forest to pasture, with initial reference to northern Costa Rica. Technical Report. VU University, Amsterdam and Aylesford, UK: Forestry Research Program of the UK Department for International Development, http://www.falw.vu/~fiesta/.

Bruijnzeel, L.A., Eugster, W., Burkard, R., 2005. Fog as a hydrologic input, in: Anderson, M.G. (Ed.), Encyclopaedia of Hydrological Sciences. John Wiley & Sons, Chichester, pp. 559–582.

Bruijnzeel, L.A., Mulligan, M., Scatena, F.N., 2011. Hydrometeorology of tropical montane cloud forests: emerging patterns. Hydrol. Process. 25, 465–498.

Calder, I.R., Kidd, C.H.R., 1978. A note on the dynamic calibration of tipping-bucket gauges. J. Hydrol. 39, 383–386.

Cavelier, J., Goldstein, G., 1989. Mist and fog interception in elfin cloud forests in colombia and venezuela. J. Trop. Ecol. 5, 309–322.

Crockford, R.H., Richardson, D.P., 2000. Partitioning of rainfall into throughfall, stemflow and interception: effect of forest type, ground cover and climate. Hydrol. Process. 14, 2903–2920.

Darwin, C., 1859. On the origin of species by means of natural selection, or the preservation of favoured races in the struggle for life. The complete work of Charles Darwin Online, http://darwin-online.org.uk.

Domingo, F., Sánchez, G., Moro, M.J., Brenner, A.J., Puigdefábregas, J., 1998. Measurement and modelling of rainfall interception by three semi-arid canopies. Agr. Forest Meteorol. 91, 275 – 292.

Domínguez González, C., 2011. Análisis de la variabilidad espacial y temporal de la trascolación en la isla Santa Cruz. Master's thesis. Escuela Politécnica Nacional, Facultad de ingeniería civil y ambiental, Quito, Ecuador, http://bibdigital.epn.edu.ec/handle/15000/3982.

d'Ozouville, N., 2007a. Agua dulce: la realidad de un recurso crítico. Informe Galápagos 2006-2007 , 150–160.

d'Ozouville, N., 2007b. Etude du Fonctionnement Hydrologique Dans les Iles Galápagos : caractérisation d'un milieu volcanique insulaire et préalable à la gestion de la ressource. Ph.D. thesis. Université Paris 6 Pierre et Marie Curie.

d'Ozouville, N., Deffontaines, B., Benveniste, J., Wegmüller, U., Violette, S., de Marsily, G., 2008. DEM generation using ASAR (ENVISAT) for addressing the lack of freshwater ecosystems management, Santa Cruz Island, Galapagos. Remote Sens. Environ. 112, 4131–4147.

Dunkerley, D., 2010. A new method for determining the throughfall fraction and throughfall depth in vegetation canopies. J. Hydrol. 385, 65 – 75.

Dykes, A.P., 1997. Rainfall interception from a lowland tropical rainforest in Brunei. J. Hydrol. 200, 260 – 279.

Eden, C., Timmermann, A., 2004. The influence of the Galapagos Islands on tropical temperatures, currents and the generation of tropical instability waves. Geophysical Res. Lett. 31, L15308.

Eugster, W., Burkard, R., Holwerda, F., Scatena, F.N., Bruijnzeel, L.A., 2006. Characteristics of fog and fogwater fluxes in a Puerto Rican elfin cloud forest. Agr. Forest Meteorol. 139, 288–306.

Foster, P., 2001. The potential negative impacts of global climate change on tropical montane cloud forests. Earth-Sci. Rev. 55, 73 – 106.

Frumau, K.F., Bruijnzeel, L.A., Tobón, C., 2011. Precipitation measurement and derivation of precipitation inclination in a windy mountainous area in northern Costa Rica. Hydrol. Process. 25, 499–509.

Frumau, K.F.A., Bruijnzeel, L.A., Tobón, C., 2006. Hydrological measurement protocol for montane cloud forest. Annex 2, Final Technical Report DFID-FRP Project R7991. Technical Report. VU University, Amsterdam and Aylesford, UK: Forestry Research Program of the UK Department for International Development, http://www.falw.vu/~fiesta/.

Gabriel, G., Jauze, L., 2008. Fog water interception by Sophora denudata trees in a Reunion upper-montane forest, Indian Ocean. Atmos. Res. 87, 338–351.

García-Santos, G., 2007. An ecohydrological and soils study in a montane cloud forest in the National Park of Garajonay, La Gomera (Canary Islands, Spain). Ph.D. thesis. PhD Thesis, VU University Amsterdam, Amsterdam, The Netherlands.

García-Santos, G., Bruijnzeel, L.A., 2011. Rainfall, fog and throughfall dynamics in a subtropical ridge top cloud forest, National Park of Garajonay (La Gomera, Canary Islands, Spain). Hydrol. Process. 25, 411–417.

Gash, J.H.C., 1979. Analytical model of rainfall interception by forests. Q. J. Roy. Meteorol. Soc. 105, 43–55.

Gash, J.H.C., Morton, A.J., 1978. An application of the Rutter model to the estimation of the interception loss from Thetford forest. J. Hydrol. 38, 49–58.

Gash, J.H.C., Valente, F., David, J.S., 1999. Estimates and measurements of evaporation from wet, sparse pine forest in Portugal. Agr. Forest Meteorol. 94, 149 – 158.

Giambelluca, T.W., DeLay, J.K., Nullet, M.A., Scholl, M.A., Gingerich, S.B., 2011. Canopy water balance of windward and leeward Hawaiian cloud forests on Haleakalā, Maui, Hawai'i. Hydrol. Process. 25, 438–447.

Giambelluca, T.W., Fox, J., Yarnasarn, S., Onibutr, P., Nullet, M.A., 1999. Dry-season radiation balance of land covers replacing forest in northern Thailand. Agr. Forest Meteorol. 95, 53 – 65.

Giambelluca, W.T., Nullet, D., 1991. Influence of the trade-wind inversion on the climate of a leeward mountain slope in Hawaii. Clim. Res. 1, 207–216.

Hafkenscheid, R.L.L.J., Bruijnzeel, L.A., M., D.J.R.A., J., B.N., 2002. Water Budgets of two upper montane rain forests of contrasting stature in the Blue Mountains, Jamaica, in: Proceedings of the Second International Colloquium on Hydrology and Water Management. Gladwell JS (ed). Cathalac: Panamá City, Panamá.

Hamann, O., 1979. On climatic conditions, vegetation types, and leaf size in the Galapagos Islands. Biotropica 11, 101–122.

Hölscher, D., Köhler, L., van Dijk, A.I.J.M., Bruijnzeel, L.A., 2004. The importance of epiphytes to total rainfall interception by a tropical montane rain forest in Costa Rica. J. Hydrol. 292, 308 – 322.

Holwerda, F., 2005. Water and energy budgets of rain forests along an elevation gradient under maritime tropical conditions. Ph.D. thesis. Vrije Universiteit Amsterdam.

Holwerda, F., Bruijnzeel, L.A., Munoz-Villers, L.E., Equihua, M., Asbjornsen, H., 2010a. Rainfall and cloud water interception in mature and secondary lower montane cloud forests of central Veracruz, Mexico. J. Hydrol. 384, 84–96.

Holwerda, F., Bruijnzeel, L.A., Oord, A.L., Scatena, F.N., 2010b. Fog interception in a puerto rican elfin cloud forest: a wet-canopy water budget approach, in: Bruijnzeel, L., F.N., S., L.S., H. (Eds.), Tropical Montane Cloud Forests: science for conservation and management. International hydrology series - Cambridge University Press.

Holwerda, F., Bruijnzeel, L.A., Scatena, F.N., 2011. Comparison of passive fog gauges for determining fog duration and fog interception by a Puerto Rican elfin cloud forest. Hydrol. Process. 25, 367–373.

Holwerda, F., Bruijnzeel, L.A., Scatena, F.N., Vugts, H.F., Meesters, A., 2012. Wet canopy evaporation from a puerto rican lower montane rain forest: the importance of realistically estimated aerodynamic conductance. J. Hydrol. 414-415, 1–15.

Holwerda, F., Burkard, R., Eugster, W., Scatena, F.N., Meesters, A.G.C.A., Bruijnzeel, L.A., 2006a. Estimating fog deposition at a Puerto Rican elfin cloud forest site: comparison of the water budget and eddy covariance methods. Hydrol. Process. 20, 2669–2692.

Holwerda, F., Scatena, F.N., Bruijnzeel, L.A., 2006b. Throughfall in a Puerto Rican lower montane rain forest: A comparison of sampling strategies. J. Hydrol. 327, 592 – 602.

Hutley, L.B., Yates, D.J., Doley, D., Boonsaner, A., 1997. Water balance of an Australian subtropical rainforest at altitude: the ecological and physiological significance of intercepted cloud and fog. Aust. J. Bot. 45, 311–329.

INEC-CGG, 2010. Encuesta de Condiciones de Vida 2009-2010. Technical Report. Instituto Nacional de Estadistica y Censos, Quito, Ecuador.

Jackson, I.J., 1975. Relationships between rainfall parameters and interception by tropical forest. J. Hydrol. 24, 215 – 238.

Jäger, H., Kowarik, I., Tye, A., 2009. Destruction without extinction: long-term impacts of an invasive tree species on Galápagos highland vegetation. J. Ecol. 97, 1252–1263.

Kimmins, J.P., 1973. Some statistical aspects of sampling throughfall precipitation in nutrient cycling studies in British Columbian coastal forests. Ecology 54, 1008–1019.

Klaassen, W., 2001. Evaporation from rain-wetted forest in relation to canopy wetness, canopy cover, and net radiation. Water Resour. Res. 37, 3227–3236.

Köhler, L., Tobón, C., Frumau, K., Bruijnzeel, L.A., 2007. Biomass and water storage dynamics of epiphytes in old-growth and secondary montane cloud forest stands in Costa Rica. Plant Ecol. 193, 171–184. 10.1007/s11258-006-9256-7.

Kolivras, K.N., Comrie, A.C., 2007. Regionalization and variability of precipitation in Hawaii. Phys. Geogr. 28, 76–96.

Lawton, R.O., Nair, U.S., Pielke, R.A., Welch, R.M., 2001. Climatic impact of tropical lowland deforestation on nearby montane cloud forests. Science 294, 584.

Link, T.E., Unsworth, M., Marks, D., 2004. The dynamics of rainfall interception by a

seasonal temperate rainforest. Agr. Forest Meteorol. 124, 171–191.
Liu, S.G., 2001. Evaluation of the Liu model for predicting rainfall interception in forests world-wide. Hydrol. Process. 15, 2341–2360.
Llorens, P., 1997. Rainfall interception by a Pinus sylvestris forest patch overgrown in a Mediterranean mountainous abandoned area II. Assessment of the applicability of Gash's analytical model. J. Hydrol. 199, 346 – 359.
Llorens, P., Gallart, F., 2000. A simplified method for forest water storage capacity measurement. J. Hydrol. 240, 131 – 144.
Llorens, P., Poch, R., Latron, J., Gallart, F., 1997. Rainfall interception by a Pinus sylvestris forest patch overgrown in a Mediterranean mountainous abandoned area I. Monitoring design and results down to the event scale. J. Hydrol. 199, 331 – 345.
Macfarlane, C., Hoffman, M., Eamus, D., Kerp, N., Higginson, S., McMurtrie, R., Adams, M., 2007. Estimation of leaf area index in eucalypt forest using digital photography. Agr. Forest Meteorol. 143, 176–188.
Massman, W.J., 1983. The derivation and validation of a new model for the interception of rainfall by forests. Agr. Meteorol. 28, 261 – 286.
McJannet, D., Wallace, J., Fitch, P., Disher, M., Reddell, P., 2007a. Water balance of tropical rainforest canopies in north Queensland, Australia. Hydrol. Process. 21, 3473–3484.
McJannet, D., Wallace, J., Reddell, P., 2007b. Precipitation interception in Australian tropical rainforests: I. Measurement of stemflow, throughfall and cloud interception. Hydrol. Process. 21, 1692–1702.
McJannet, D., Wallace, J., Reddell, P., 2007c. Precipitation interception in Australian tropical rainforests: II. Altitudinal gradients of cloud interception, stemflow, throughfall and interception. Hydrol. Process. 21, 1703–1718.
Monteith, J.L., 1965. Evaporation and environment. Symposia for the Society of Experimental Biology 19, 205–234.
Muzylo, A., Llorens, P., Valente, F., Keizer, J.J., Domingo, F., Gash, J.H.C., 2009. A review of rainfall interception modelling. J. Hydrol. 370, 191 – 206.
Muñoz-Villers, L.E., Holwerda, F., Gómez-Cárdenas, M., Equihua, M., Asbjornsen, H., Bruijnzeel, L.A., Marín-Castro, B.E., Tobón, C., 2011. Water balances of old-growth and regenerating montane cloud forests in central Veracruz, Mexico. J. Hydrol. In Press, Corrected Proof.
National Weather Service Climate Prediction Center, 2011. ENSO Cold and Warm Episodes by Season, http://www.cpc.ncep.noaa.gov/products/analysis_monitoring/ensostuff/ensoyears.shtml .
Návar, J., Bryan, R.B., 1994. Fitting the analytical model of rainfall interception of Gash to individual shrubs of semi-arid vegetation in northeastern Mexico. Agr. Forest Meteorol. 68, 133 – 143.
Nullet, D., Juvik, J.O., Wall, A., 1995. A Hawaiian mountain climate cross-section. Clim. Res. 5, 131–137.
Pearce, A.J., Gash, J.H.C., Stewart, J.B., 1980. Rainfall interception in a forest stand estimated from grassland meteorological data. J. Hydrol. 46, 147 – 163.
PNG, 2010. Informe Ingreso Turistas. Technical Report. Parque Nacional Galapagos.
Porter, D., 1815. Journal of a Cruise made to the Pacific Ocean, by Captain David Porter, in the United States Frigate ESSEX, in the years 1812,1813, and 1914. Bradford and

Inskeep, Philadelphia.
Prada, S., Menezes de Sequeira, M., Figueira, C., da Silva, M.O., 2009. Fog precipitation and rainfall interception in the natural forests of Madeira Island (Portugal). Agr. Forest Meteorol. 149, 1179–1187.
R Development Core Team, 2009. R: A Language and Environment for Statistical Computing. R Foundation for Statistical Computing, Vienna, Austria ISBN 3-900051-07-0.
Ritter, A., Regalado, C.M., Aschan, G., 2008. Fog water xollection in a subtropical elfin laurel forest of the Garajonay National Park (Canary Islands): a combined approach using artificial fog catchers and a physically based impaction model. J. Hydrometeorol. 9, 920–935.
Ritter, A., Regalado, C.M., Aschan, G., 2009. Fog reduces transpiration in tree species of the Canarian relict heath-laurel cloud forest (Garajonay National Park, Spain). Tree Physiol. 29, 517–528.
Rutter, A.J., Kershaw, K.A., Robins, P.C., Morton, A.J., 1972. A predictive model of rainfall interception in forests, 1. Derivation of the model from observations in a plantation of Corsican pine. Agr. Meteorol. 9, 367 – 384.
Rutter, A.J., Morton, A.J., Robins, P.C., 1975. A predictive model of rainfall interception in forests. II. Generalization of the model and comparison with observations in some coniferous and hardwood stands. J. Appl. Ecol. 12, 367–380.
Sachs, J.P., Ladd, S.N., 2010. Climate and oceanography of the Galapagos in the 21st century: expected changes and research needs. Galapagos Res. 67, 50–54.
Scatena, F.N., 1990. Watershed scale rainfall interception on two forested watersheds in the Luquillo Mountains of Puerto Rico. J. Hydrol. 113, 89 – 102.
Scatena, F.N., Bruijnzeel, L., Bubb, P., Das, S., 2010. Setting the stage, in: L.A., B., F.N., S., L.S., H. (Eds.), Tropical Montane Cloud Forests: science for conservation and management. International Hydrology Series - Cambridge University Press.
Schellekens, J., Bruijnzeel, L.A., Scatena, F.N., Bink, N.J., Holwerda, F., 2000. Evaporation from a tropical rain forest, Luquillo Experimental Forest, eastern Puerto Rico. Water Resour. Res. 36, 2183–2196.
Schellekens, J., Scatena, F.N., Bruijnzeel, L.A., Wickel, A.J., 1999. Modelling rainfall interception by a lowland tropical rain forest in northeastern Puerto Rico. J. Hydrol. 225, 168 – 184.
Sharon, D., 1980. The distribution of hydrologically effective rainfall incident on sloping ground. J. Hydrol. 46, 165–188.
Snell, H.L., Rea, S., 1999. Thet 1997-98 El Niño in Galapagos: can 34 years of data estimate 120 years of pattern. Noticias de Galápagos 60.
Stadtmüller, T., 1987. Cloud Forests in the Humid Tropics: a bibliographic review. CATIE, Turrialba, Costa Rica.
Staelens, J., Schrijver, A.D., Verheyen, K., Verhoest, N.E., 2006. Spatial variability and temporal stability of throughfall water under a dominant beech (Fagus sylvatica L.) tree in relationship to canopy cover. J. Hydrol. 330, 651 – 662.
Still, C.J., Foster, P.N., Schneider, S.H., 1999. Simulating the effects of climate change on tropical montane cloud forests. Nature 398, 608–610.
Takahashi, M., Giambelluca, T.W., Mudd, R.G., DeLay, J.K., Nullet, M.A., Asner, G.P., 2011. Rainfall partitioning and cloud water interception in native forest and invaded forest in Hawai'i Volcanoes National Park. Hydrol. Process. 25, 448–464.

Thimonier, A., 1998. Measurement of atmospheric deposition under forest canopies: some recommendations for equipment and sampling design. Environ. Monit. and Assess. 52, 353–387.

Trueman, M., d'Ozouville, N., 2010. Characterizing the Galapagos terrestrial climate in the face of global climate change. Galapagos Res. 67, 26–37.

Valente, F., David, J.S., Gash, J.H.C., 1997. Modelling interception loss for two sparse eucalypt and pine forests in central Portugal using reformulated Rutter and Gash analytical models. J. Hydrol. 190, 141–162.

Villegas, C., Tobón, C., Breshears, D.D., 2008. Fog interception by non-vascular epiphytes in tropical montane cloud forests: dependencies on gauge type and meteorological conditions. Hydrol. Process. 22, 2484–2492.

Wallace, J., McJannet, D., 2006. On interception modelling of a lowland coastal rainforest in northern Queensland, Australia. J. Hydrol. 329, 477–488.

Weathers, K.C., Lovett, G.M., Likens, G.E., 1995. Cloud deposition to a spruce forest edge. Atmos. Environ. 29, 665 – 672.

Ziegler, A.D., Giambelluca, T.W., Nullet, M.A., Sutherland, R.A., Tantasarin, C., Vogler, J.B., Negishi, J.N., 2009. Throughfall in an evergreen-dominated forest stand in northern Thailand: Comparison of mobile and stationary methods. Agr. Forest Meteorol. 149, 373 – 384.

Zimmermann, B., Zimmermann, A., Lark, R.M., Elsenbeer, H., 2010. Sampling procedures for throughfall monitoring: A simulation study. Water Resour. Res. 46, W01503.